Received 10 March 2017; revised 30 April 2017; accepted 9 May 2017. Date of publication 15 May 2017;
date of current version 21 June 2017. The review of this paper was arranged by Editor C. C. McAndrew.

Digital Object Identifier 10.1109/JEDS.2017.2704106

A Unified Continuous and Discrete Model for Double-Gate MOSFETs With Spatially Varying or Pulsed Doping Profiles

CHUYANG HONG[1], JUN ZHOU[1], QI CHENG[1], KUNKUN ZHU[1], JAMES B. KUO[2] (Fellow, IEEE), AND YIJIAN CHEN[1] (Member, IEEE)

1 School of Electronic and Computer Engineering, Shenzhen Graduate School, Peking University, Shenzhen 518055, China
2 Department of Electrical Engineering, National Taiwan University, Taipei, Taiwan

CORRESPONDING AUTHOR: Y. CHEN (e-mail: chenyj@pkusz.edu.cn)

This work was supported in part by the National Natural Science Foundation of China under Grant 61574002, in part by the Natural Science Foundation of Guangdong Province, China under Grant 1414050004175, and in part by the Shenzhen City's Strategic Development Fund for Fundamental Research under Grant JCYJ20150630152545236.

ABSTRACT This paper presents a unified continuous and discrete model covering all device operating regions of double-gate MOSFETs for the first time. With a specific variable transformation method, the 1-D Poisson's equation in the Cartesian coordinate for double-gate MOSFETs is transformed into the corresponding form in the cylindrical coordinate. Such a transformed cylindrical Poisson's equation results in a simple algebraic equation, which correlates the (inversion-charge induced) surface potential to the field and allows the long-channel drain-current formula to be derived from the Pao–Sah integral. This model can be readily applied to predict the effects of both continuous and discrete doping variations. The short-channel-effect model is also developed by solving the 2-D Poisson's equation using the eigenfunction-expansion method. The accuracy of both long-channel and short-channel models is confirmed by the numerical calculations and TCAD simulations.

INDEX TERMS Double-gate MOSFET/FinFET, surface-field based model, discrete dopant variations.

I. INTRODUCTION

Double-gate MOSFET has been adopted in the past as the mainstream structure of logic devices to replace the conventional planar MOSFETs to achieve improved control of the short-channel effects [1]–[5]. For more than a decade, double-gate MOSFET modeling had remained a particularly active research area and various types of double-gate MOSFET models were already reported [6]–[30]. Several groups developed compact models for undoped double-gate MOSFETs by solving the 1-D Poisson's equation which contains only the mobile-charge term [6]–[14]. Some approaches such as PSP-Based [6] and EKV [7] FinFET models were constructed using the charge-sheet approximation, which may cause significant errors in the intermediate region, thus incapable of accurately describing the full device behavior. Moreover, a simple linear relation between the inversion charges and the surface potential is employed in [6], which may prevent the model from a consistent solution for all regions of device operation. Many double-gate MOSFET models are based on the rigorous solution of undoped Poisson's equation and are often referred to as the potential-based [8]–[10] or the charge-based [11], [12] models. However, the device channel is often doped and no analytical solution was reported for the doped Poisson's equation. Various types of approximation are therefore needed to describe the nonlinear interaction between the mobile and the depletion charges [14]–[21]. Typical treatments include the superposition or perturbation method [14], [15], and an iterative approximation [16]. These methods can provide high accuracy only when the nonlinear interaction mentioned above is weak. Some other models adopt physical intuition based approximations such as the fully depletion [17], [18] or the moderate inversion approximations [19], which may result in a low accuracy in the uncovered regions. Considering the discrete nature of the practical doping profiles and the compatibility

with the conventional models, a unified model covering both continuous and discrete doping profiles is highly desirable.

Recently, a surface-field-based drain current model has been proposed for nanowire MOSFETs with continuous [31] and discrete doping profiles [32]. By introducing a variable transformation method, the doping related effects were lumped into the mobile-charge term. Without solving the explicit potential distribution, an algebraic relation between the surface potential and the field was derived to calculate the drain current using the Pao-Sah integral. The first challenge to extend this method to double-gate MOSFET modeling is that the specific variable transformation for Poisson's equation in the cylindrical coordinate does not work for the Cartesian system, which is needed for describing the double-gate MOSFETs. Naturally, our double-gate MOSFET modeling approach is to transform Poisson's equation in the Cartesian coordinate into the corresponding form in the cylindrical system [33]. After that, the variable transformation method applicable to the cylindrical Poisson's equation [31], [32], [34] can be employed, although the boundary conditions must be modified accordingly. Secondly, how to estimate the central potential used to be the bottleneck when solving the potential solution of doped double-gate MOSFETs and various types of approximations were required. Although an algebraic equation can be derived to correlate the surface potential to field of a double-gate MOSFET [31]–[34], this difficulty still remains and a full-regime approximation must be searched. In our model development, an accurate formula for all device operating regions will be derived by constructing a smoothing function to correlate the central potential to the surface field. By overcoming the above challenges for both continuous and discrete doping profiles, we extend our previous work and develop a unified double-gate MOSFET model capable of predicting the effect of both continuous and discrete dopant variations.

Moreover, the short-channel effect is studied by applying the eigenfunction-expansion method to solve the 2-D Poisson's equation for devices with continuous and discrete doping distributions. Key device parameters such as the threshold voltage, threshold voltage roll-off and subthreshold current are calculated from the short-channel model and compared with TCAD simulations results. An excellent agreement between them is found.

II. SURFACE-FIELD-BASED CORE MODEL DEVELOPMENT

A. SURFACE-FIELD-BASED MODEL

A double-gate MOSFET with an n-type channel is shown in Figure 1. The 1-D Poisson's equation considering both the depletion and the inversion charges is written as:

$$\frac{\partial^2\varphi}{\partial x^2} = \frac{qn_i{}^2}{\varepsilon_{si}N_a}\cdot e^{\frac{q[\varphi-V(y)]}{kT}} + \frac{qN_a(x)}{\varepsilon_{si}}, \qquad (1)$$

where $\varphi(x, y)$ is the potential, $N_a(x)$ is a spatially varying doping distribution in the silicon channel and can be either

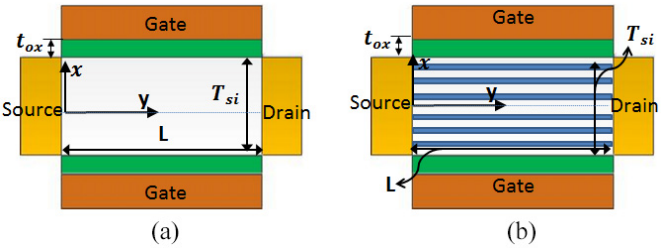

FIGURE 1. Schematic description of a double-gate MOSFET with a 1-D (a) continuous or (b) discrete doping profile. Both doping concentrations are assumed to be independent of y (channel direction), and only varying in the x direction while symmetric with respect to x=0.

continuous or discrete (e.g., Dirac δ functions to describe the discrete dopant variations), and $V(y)$ is the electron quasi-Fermi potential. The standalone doping term $qN_a(x)/\varepsilon_{si}$ is removed by introducing a new variable $Z(x)$:

$$\varphi(x, y) = \frac{kT}{q}Z(x) + V(y) + g(x).$$

where $g(x)$ is a spatial function which satisfies:

$$\frac{d^2g(x)}{dx^2} = \frac{qN_a(x)}{\varepsilon_{si}}.$$

Substituting the above equation into Eq. (1) yields:

$$\frac{d^2Z}{dx^2} = \left(\frac{q^2n_i^2}{kT\varepsilon_{si}}\right)\cdot\left[\frac{e^{\frac{q}{kT}g(x)}}{N_a}\right]\cdot e^Z = \xi\cdot f(x)\cdot e^Z, \qquad (2)$$

where $\xi = q^2n_i^2/(kT\varepsilon_{si})$ and $f(x) = Exp[qg(x)/kT]/N_a$ contains the effect of nonlinear coupling between the inversion and the depletion charges. The introduced coupling function $f(x)$ is where our model differs from many existing double-gate MOSFET models. It can be either a continuous (for continuous doping profiles) or discrete function (i.e., mathematically treated as Dirac δ functions for discrete doping profiles [31], [32]). Although Eq. (2) appears simpler than its corresponding form in the cylindrical coordinate, the reported variable transformation method, that specifically works for cylindrical nanowire MOSFETs [31], is invalid for transforming Eq. (2) into a manageable form. However, by introducing two specific variables $Z_C = Z - 2\ln\tau$ and $\tau = e^x$ [33], Eq. (2) can be transformed into a form similar to the doped Poisson's equation in the cylindrical coordinate [31]:

$$\frac{d^2Z_C}{d\tau^2} + \frac{1}{\tau}\frac{dZ_C}{d\tau} = \xi\cdot f(\ln\tau)\cdot e^{Z_C} = \xi\cdot F(\tau)\cdot e^{Z_C}, \qquad (3)$$

where $F(\tau) = f(ln\tau)$. Eqs. (2) and (3) indicate that Poisson's equations in both Cartesian and cylindrical coordinates can be transformed into each other. The theoretical significance of this characteristic is evident, especially for undoped (or lightly doped) multi-gate MOSFETs. For instance, the general solution (in the real domain) of nonlinear Poisson's equation in one coordinate system can be readily derived based on the solution in the other coordinate. In the Appendix, we show the complete three-branch general

solution of undoped 1-D Poisson's equation in both Cartesian and cylindrical coordinates, which indicates that the existing cylindrical solution reported in the MOSFET device literature is incomplete, i.e., only suitable for certain boundary condition (e.g., the zero field at the center of a nanowire channel). Apparently, the complete general solution of nonlinear Poisson's equation should be known in order to explore other types of emerging transistor structures (e.g., double-surrounding-gate nanoshell MOSFET) with different boundary conditions.

The above transformation allows us to apply the more convenient surface-field approach for gate-all-around (GAA) nanowire MOSFETs [31], [32], [34] to model double-gate MOSFETs. For this purpose, two new variables are introduced:

$$\beta = \tau \frac{dZ_C}{d\tau}, \eta = \tau^2 F(\tau) Exp(Z_C).$$

Equation (3) is then further transformed to:

$$d\beta \left[\beta + p(\tau)\right] = \xi \cdot d\eta, \tag{4}$$

where $p(\tau) = 2 + \tau F'(\tau)/F(\tau)$ is a spatial function only related with the doping profile as shown in Figure 2. Assuming a symmetric doping and potential distribution, we shall only consider the half part of the channel and integrate Eq. (4) from the center to one surface (i.e., $\tau = \epsilon_+ = Exp(T_{si}/2)$):

$$\frac{\beta_s^2}{2} - \frac{\beta_0^2}{2} + \int_{\beta_0}^{\beta_s} p\left[\tau(\beta)\right] d\beta = \frac{\beta_s^2}{2} - \frac{\beta_0^2}{2} + M = \xi\left(\eta_s - \eta_0\right), \tag{5}$$

where $M = \int_{\beta_0}^{\beta_s} p[\tau(\beta)]d\beta = \int_1^{\epsilon_+} [p(\tau)d\beta/d\tau]d\tau$ is an integral to be determined. The subscripts "*0*" and "*s*" stand for the values at the center (i.e., $\tau = 1 = Exp(0)$) and on the surface of the channel, respectively. Here, we consider a symmetric device such that $\beta_0 = 1 \cdot (dZ/d\tau)|_{\tau=1} - 2 = -2$ is required. Note that no approximation is made in the above derivation, which means that Eq. (5) is rigorously valid for any symmetric type (continuous or discrete) of doping profile. However, two undetermined factors M and η_0 (η_0 is a parameter related with the doping concentration and the electric potential at the channel center) need to be solved using certain approximations.

B. APPROXIMATION OF FACTOR M

Note that $p(\tau)$ in Eq. (5) is a dimensionless function as in a surface-field based GAA nanowire MOSFET model [31]. When a double-gate MOSFET is undoped, $p(\tau)$ will degenerate to two, which is the same case as an undoped GAA nanowire MOSFET. For doped devices, the value of $p(\tau)$ at the center (i.e., $\tau = 1 = Exp(0)$) will also approach two, as shown by some examples in Figure 2. Treating $p(\tau)$ as a constant has been demonstrated to be highly accurate for deep nanoscale devices with a low-to-medium doping level [31], [34]. In order to calculate the

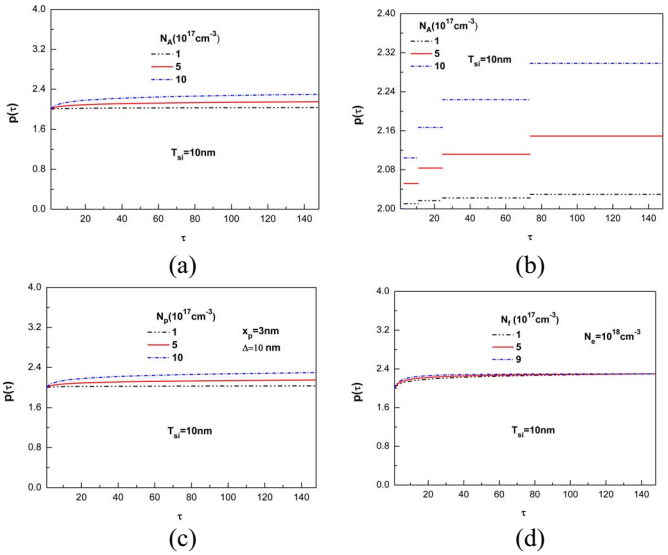

FIGURE 2. Examples of $p(\tau)$ of DG MOSFETs as a function of τ for (a) uniformly doped profiles with varying concentrations, (b) discrete doping profiles with varying N_A, (c) Gaussian doping profiles with varying N_p, (d) cosine-function doping profiles with varying N_f. Note that a Gaussian doping profile is defined as: $N_a(x) = N_p \exp[-(x - R_p)^2/2\Delta^2]$, and a cosine-function doping profile is defined as: $N_a(x) = N_e + N_f \cos(\pi x/R)$.

M integral, the explicit form of $d\beta/d\tau$ needs to be known. To derive the approximate formula of $d\beta/d\tau$, $p(\tau)$ will be treated as a constant and Eq. (4) can be readily integrated to obtain:

$$\frac{\beta^2}{2} + p\beta - h \approx \xi\eta, \tag{6}$$

where $h = -\xi\eta_0 + p\beta_0 + \beta_0^2/2 = -\xi\eta_0 - 2p + 2$ is an integration constant to be determined from the boundary condition. Substituting $\beta = \tau dZ_C/d\tau$ and $\eta = \tau^2 F(\tau) Exp(Z_C)$ into Eq. (6) and using Eq. (3) to remove the exponential term yields:

$$\frac{d^2 Z_C}{d\tau^2} - \frac{(p-1)}{\tau}\frac{dZ_C}{d\tau} - \frac{1}{2}\left(\frac{dZ_C}{d\tau}\right)^2 + \frac{h}{\tau^2} \approx 0. \tag{7}$$

Eq. (7) can be analytically solved to obtain a general solution:

$$Z_C \approx -p\ln\tau + A - 2\ln\left|\cos\left(\frac{1}{2}\sqrt{-(p-2)^2 - 2h}\ln\tau - B\sqrt{-(p-2)^2 - 2h}\right)\right|, \tag{8}$$

where A and B are two integration constants. Hence $\beta(\tau)$ can be approximated as:

$$\beta(\tau) \approx -p + \sqrt{-(p-2)^2 - 2h}\tan\left[\frac{1}{2}\sqrt{-(p-2)^2 - 2h}\ln\tau - B\sqrt{-(p-2)^2 - 2h}\right]. \tag{9}$$

On the channel surface ($\tau = \epsilon_+$), β_s is estimated as:

$$\beta_s \approx -p + \sqrt{-(p-2)^2 - 2h}\tan\left[\frac{1}{2}\sqrt{-(p-2)^2-2h}\ln\epsilon_+ - B\sqrt{-(p-2)^2-2h}\right]. \quad (10)$$

Using Eq. (10), the unknown constant B in (9) can be replaced by β_s:

$$\beta(\tau) \approx -p + \sqrt{-(p-2)^2-2h}\tan\left\{\frac{1}{2}\sqrt{-(p-2)^2-2h}\,(\ln\tau - \ln\epsilon_+) + \arctan\left[\frac{\beta_s + p}{\sqrt{-(p-2)^2-2h}}\right]\right\}. \quad (11)$$

It should be reminded that although Eq. (11) provides a highly accurate approximation of the electric-field related function $\beta(\tau)$ by assuming a constant $p(\tau)$, it is only used to estimate $d\beta/d\tau$ when calculating the M integral. On the other hand, $p(\tau)$ in the M integral of Eq. (5) will remain its exact form (i.e., a spatial function rather than a constant) such that our model is not limited to the above constant $p(\tau)$ approximation. To predict the on-state current, this constant (p) is chosen to be the surface value of $p(\tau)$.

Compared with the surface-field based GAA nanowire MOSFET model [31], the challenging task for double-gate MOSFET modeling is that the integration constant h in Eqs. (6) and (11) needs to be determined from the central potential while the potential distribution along the channel is still unknown. Naturally, the next step is to estimate η_0 by making further approximations.

C. ESTIMATION OF FACTOR η_0

To approximately calculateη_0, we shall first make a first-order approximation wherein a uniform doping concentration N_A is assumed. Note that the assumption of a uniform doping profile is only used to estimate η_0, while the influence of doping variations will be reflected by keeping the spatially varying function $p(\tau)$ in the M integral of Eq. (5). The total dopant number in the channel with such a uniform doping profile is set to be equal to that with the exact (spatially varying) doping profile.

By this treatment, Eq. (1) can be simplified to a well-known form of 1-D Poisson's equation, which is the governing equation of many FinFET compact models:

$$\frac{\partial^2\varphi_a}{\partial x^2} = \frac{qn_i{}^2}{\varepsilon_{si}N_A}\cdot e^{\frac{q[\varphi_a - V(y)]}{kT}} + \frac{qN_A}{\varepsilon_{si}}, \quad (12)$$

where φ_a stands for the first-order approximation of potential. In the sub-threshold region, φ_a can be analytically solved by neglecting the mobile charge term:

$$\varphi_a(x,y) = \frac{qN_A}{\varepsilon_{si}}\frac{x^2}{2} + \varphi_a(0,y). \quad (13)$$

Eq. (13) allows us to approximately calculate the total mobile charge density (per unit area) in the sub-threshold region [35], [36]:

$$Q_m = \int_0^{\frac{T_{si}}{2}} \frac{qn_i^2}{N_a} e^{\frac{q[\varphi_a(x,y) - V(y)]}{kT}} dx = e^{\frac{q}{kT}[\varphi_a(0,y) - V(y)]}\theta_s, \quad (14)$$

where

$$\theta_s = \int_0^{\frac{T_{si}}{2}} \frac{qn_i^2}{N_A} e^{\frac{q(\frac{qN_A}{\varepsilon_{si}}\frac{x^2}{2})}{kT}} dx.$$

Note that $\varphi_a(0,y) \approx \varphi(0,y) = kTZ(0)/q + V(y) = kTZ_C(1)/q + V(y)$, and consequently Eq. (14) yields a linear relation between Q_m and η_0:

$$Q_m = e^{Z_C(1)}\theta_s = \frac{\eta_0}{F(1)}\theta_s. \quad (15)$$

Since $\beta(\tau)$ is directly related with the mobile-charge induced electric field, Gauss's Law requires:

$$Q_m = \varepsilon_{si}\frac{kT}{q}\frac{dZ}{dx}\bigg|_{x=\frac{T_{si}}{2}} = \varepsilon_{si}\frac{kT}{q}\left(\tau\frac{dZ_C}{d\tau}\bigg|_{\tau=\epsilon_+} + 2\right) = \frac{\varepsilon_{si}kT}{q}(\beta_s + 2). \quad (16)$$

Substituting Eq. (16) into (15) yields a simple relation between η_0 and β_s in the sub-threshold region:

$$\eta_0 = \varepsilon_{si}\frac{kTF(1)}{q\theta_s}(\beta_s + 2) = \frac{c(\beta_s + 2)}{\xi}, \quad (17)$$

where $c = \xi\varepsilon_{si}kTF(1)/(q\theta_s)$. Eq. (17) indicates the potential related parameter η_0 is a linear function of β_s. This is consistent with our physical intuition that the sub-threshold leakage occurs mainly along the path of channel center and the inversion charge density can be estimated as an exponential function of the sub-threshold channel central potential. However, it is inappropriate to extend Eq. (17) to the full region of device operation [37], e.g., η_0 remains almost unchanged when a device enters the strong inversion region and the surface potential becomes "pinned". In other words, the central potential in strong inversion exhibits a saturation behavior (insensitive to the gate voltage) due to the screening effect of inversion charge [27], [37], [38]. For a device with a uniform doping profile, the saturation value of $Z_C(1)$ is approximated as [27]:

$$Z_{Csat} = Z_{sat} \approx 2\ln\left(\frac{N_A}{n_i}\right) - \ln\left[1 - \exp(-2\alpha)\right] - \alpha + 1.6, \quad (18)$$

where Z_{sat} is the saturation value of $Z(0)$ and $\alpha = q^2N_AT_{si}{}^2/8\varepsilon_{si}kT$. As a result, the saturation value of η_0 is obtained as:

$$\eta_{0sat} = 1\cdot F(1)\,Exp(Z_{Csat}). \quad (19)$$

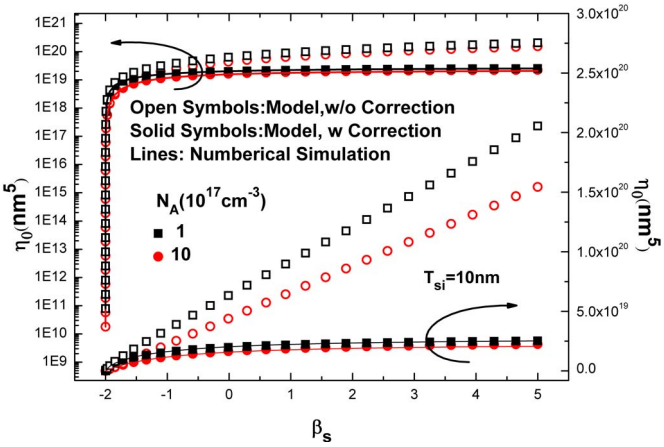

FIGURE 3. η_0 as a function of β_s for devices with a uniform doping profile.

To yield a continuous transition between these two regions, a smoothing function for η_0 is constructed:

$$\eta_0 = \frac{c(\beta_s + 2)}{\xi\left[1 + \left(\frac{\beta_s+2}{\beta_c+2}\right)^{n_c}\right]^{\frac{1}{n_c}}}, \tag{20}$$

where n_c is a parameter to control the transition smoothness (n_c is set to 1 in this paper), $\beta_c = \xi\eta_{0sat}/c - 2$. From Eq. (17), β_c is the value of β_s when η_0 reaches the saturation value η_{0sat}. As shown in Eq. (16), $(\beta_s + 2)$ is the surface field due to the mobile charge. It is well known that the mobile-charge induced surface field in subthreshold region is much lower than when the surface potential begins to be "pinned" (i.e., $(\beta_s - 2) \ll (\beta_c - 2)$). However, this subthreshold relation is no longer valid when the device enters the strong inversion region. The mobile-charge induced surface field increases rapidly with the gate voltage so that a different relation $(\beta_s - 2) \gg (\beta_c - 2)$ holds in the strong inversion region. Hence, in the subthreshold region, $(\beta_s + 2/\beta_c + 2)^{n_c} \ll 1$ and consequently$\eta_0 = \eta_{0sub} \approx c(\beta_s + 2)/\xi$; in the strong inversion region, $(\beta_s + 2/\beta_c + 2)^{n_c} \gg 1$ which results in $\eta_0 = \eta_{0inv} \approx c(\beta_c + 2)/\xi$. Eq. (20) is more general than Eq. (17) since it describes both the sub-threshold and saturation behavior of the central potential. Figure 3 shows η_0 versus β_s curves calculated using Eqs. (20) and (17), respectively. Compared with numerical results [40], it is evident that the formula with the saturation correction (i.e., Eq. (20)) agrees much better with the numerical results. As a summary, Eqs. (11) and (20) can accurately predict the full-regime M and η_0 in Eq. (5).

D. DERIVATION OF DRAIN CURRENT

Another relation between the surface potential and the field is given by the oxide interface boundary condition:

$$C_{ox}\left[V_g - V_{fb} - \varphi\left(\frac{t_{si}}{2}\right)\right] = \varepsilon_{si}\left.\frac{\partial\varphi}{\partial x}\right|_{x=\frac{T_{si}}{2}}, \tag{21}$$

where V_{fb} is the flat-band voltage and $C_{ox} = \varepsilon_{ox}/T_{ox}$ is the oxide capacitance (per unit gate area). Applying the relation between φ and Z_C, Eq. (21) is rewritten as:

$$C_{ox}\left[V_g - V_{fb} - \frac{kT}{q}Z_C(\epsilon_+) - 2\frac{kT}{q}\ln\epsilon_+ - V - G(\epsilon_+)\right] = \varepsilon_{si}\epsilon_+\left[\frac{kT}{q}\left(\left.\frac{\partial Z_C}{\partial\tau}\right|_{\tau=\epsilon_+} + \frac{2}{\epsilon_+}\right) + G'(\epsilon_+)\right], \tag{22}$$

where $G(\tau) = g(\ln\tau)$. For a given V_g, β_s can be solved by coupling Eqs. (5) with (22):

$$C_{ox}\left\{V_g - V_{fb} - \frac{kT}{q}\ln\left[\frac{\frac{\beta_s^2}{2} - 2 + M + \xi\eta_0}{\xi R^2 F(\epsilon_+)}\right] - 2\frac{kT}{q}\ln\epsilon_+ - V - G(\epsilon_+)\right\} = \varepsilon_{si}\epsilon_+\left[\frac{kT}{q}\left(\frac{\beta_s + 2}{\epsilon_+}\right) + G'(\epsilon_+)\right]. \tag{23}$$

From Eq. (23), the value of β_s at the source and drain terminals $\beta_{s,s}$ and $\beta_{s,d}$ can be calculated by substituting $V = 0$ and $V = V_d$ into the equation, respectively. By differentiating Eq. (23), we obtain:

$$\frac{dV}{d\beta_s} = -\frac{kT}{q}\left(\frac{\beta_s + \frac{dM}{d\beta_s} + \xi\frac{d\eta_0}{d\beta_s}}{\frac{\beta_s^2}{2} - 2 + M + \xi\eta_0} + \frac{\varepsilon_{si}}{C_{ox}}\right).$$

Carrying out the Pao-Sah integral, the drain current can be calculated by considering $dV/dy = (dV/d\beta_s)(d\beta_s/dy)$ and $Q_m(\beta_s) = \varepsilon_{si}kT(\beta_s + 2)/q$ as a function of β_s:

$$I_{ds} = \frac{2\mu W}{L}\int_{\beta_{s,s}}^{\beta_{s,d}} Q_m(\beta_s)\frac{dV}{d\beta_s}d\beta_s, \tag{24}$$

where W is the height of the fin.

III. RESULTS AND DISCUSSION

A. RESULTS FOR CONTINUOUS DOPING PROFILES

For a double-gate MOSFET with a continuous doping distribution, the spatial function $g(x)$ is chosen as:

$$g(x) = \frac{q}{\varepsilon_{si}}\int_0^x\int_0^x N_a(x)dxdx. \tag{25}$$

Note that the uniform doping level N_A is obtained from Eq. (25):

$$N_A = \frac{\int_0^{\frac{t_{si}}{2}} N_a(x)dx}{\left(\frac{T_{si}}{2}\right)}.$$

For the purpose of simplicity, double-gate MOSFETs with uniform doping profiles are used to verify our model accuracy. A relative error index of surface field is defined as:

$$Relative\ error = \frac{|E_{s.model} - E_{s.num}|}{E_{s.num}},$$

where $E_{s.model}$, $E_{s.num}$ are the values of the surface field obtained from our model and by rigorous numerical calculation [39]. The relative-error results are plotted in Figure 4. It shows that the maximum relative-error amplitude for the double-gate MOSFETs with continuous doping

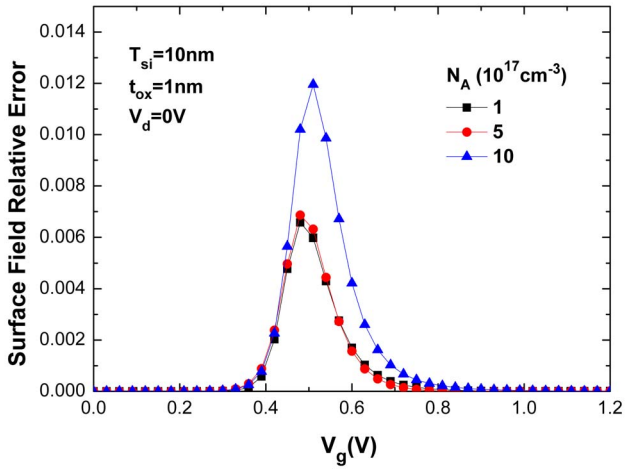

FIGURE 4. The surface field relative error as a function of V_g for devices with conventional uniform doping profiles.

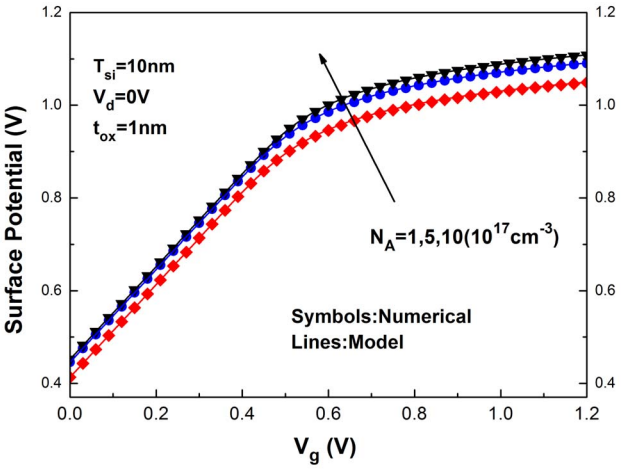

FIGURE 5. The surface electric potential as a function of V_g for devices with a uniform doping profile.

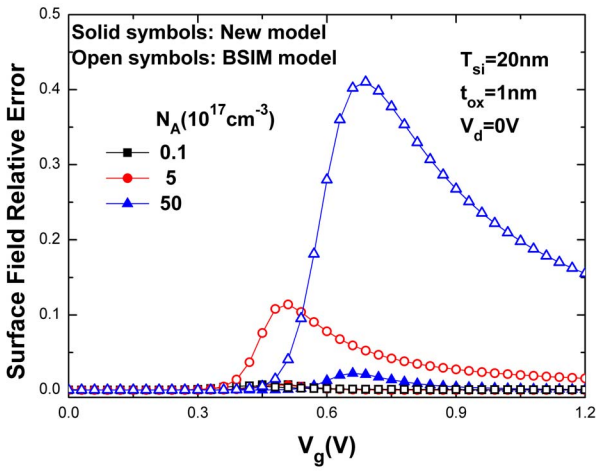

(a)

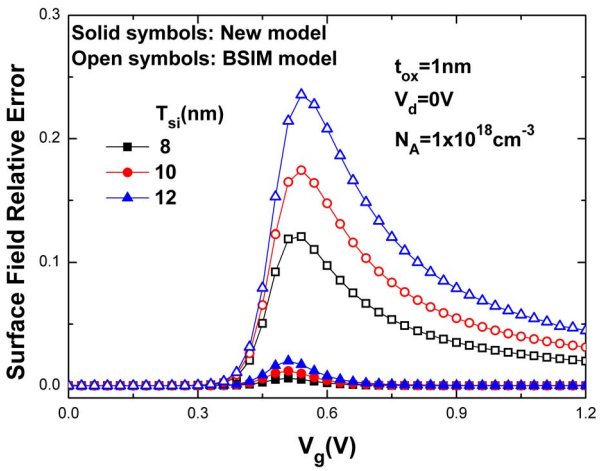

(b)

FIGURE 6. A comparison of the relative errors of surface field calculated from our new model and BSIM-CMG model for varying (a) N_A and (b) t_{si}.

profiles is lower than 1.5%, which indicates that this model is accurate for predicting the device behavior. The curves of surface potential versus gate voltage for the devices with continuous doping profiles are plotted in Figure 5. An excellent agreement with numerical calculation results is found for varying doping levels and channel thicknesses. To highlight the predicting capability of our model, we also compare the accuracy of our model with BSIM-CMG model which is a widely adopted industrial modeling platform [14]. In Figure 6, the relative-error results calculated from our model are compared with those from BSIM-CMG model. It is evident that higher accuracy is achieved by our model for a wide range of design parameters such as N_A and t_{si}.

To further verify the model accuracy, TCAD simulations based on a conventional drift-diffusion approach are carried out to investigate the impacts of key parameters on the drain current [40]. A mid-gap work function for the gate and an electron mobility of 1417 (cm^2/Vs) are assumed in this work [41]. An extensive investigation of *I-V* model accuracy for a wide range of the gate voltage, doping level, and drain voltage is conducted and the results are shown in Figure 7. The constructed smoothing function works well to predict the values of η_0 in different operating regions with high accuracy.

B. RESULTS FOR DISCRETE DOPING PROFILES

For the discrete doping profiles, 3-D Poisson's equation in Cartesian coordinate is:

$$\nabla^2\varphi\,(x,y,z) = \frac{qn_i^2}{\varepsilon_{si}N_a}\cdot e^{\frac{q[\varphi-V(y)]}{kT}} + \frac{qN_a\left(\vec{\mathbf{r}}\right)}{\varepsilon_{si}}. \quad (26)$$

The depletion-charge term in Poisson's equation is described by placing multiple Dirac δ functions in the channel:

$$N_a\left(\vec{\boldsymbol{r}}\right) = \sum_{k=1}^{n} N_k\delta\left(\vec{\boldsymbol{r}} - \vec{\boldsymbol{r_k}}\right),$$

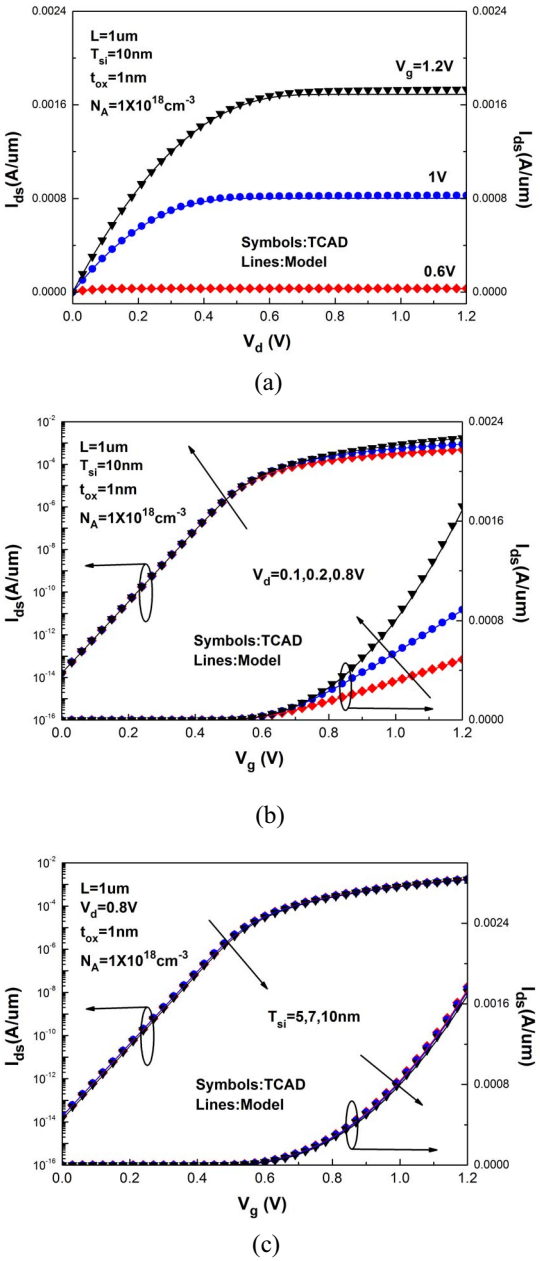

FIGURE 7. **Comparison of I_{ds} of uniformly doped double-gate MOSFETs predicted by the new model and TCAD simulations. (a) $I_{ds} - V_d$ for varying V_g, (b) $I_{ds} - V_g$ for varying V_d, (c) $I_{ds} - V_g$ for varying T_{si}.**

where n groups of dopants are distributed at n locations x_k $(k = 1, \ldots, n)$.N_k is determined by the dopant number assigned to the corresponding location. Since our focus is the long-channel model, no y- or z- dependence of the dopant distribution is considered, i.e., a discrete 1-D doping profile will be assumed. Hence, Eq. (26) can be simplified to Eq. (1) wherein the discrete depletion charges are written as:

$$N_a(x) = \sum_{k=1}^{n} \frac{N_k}{WL} \delta\,(x - x_k).$$

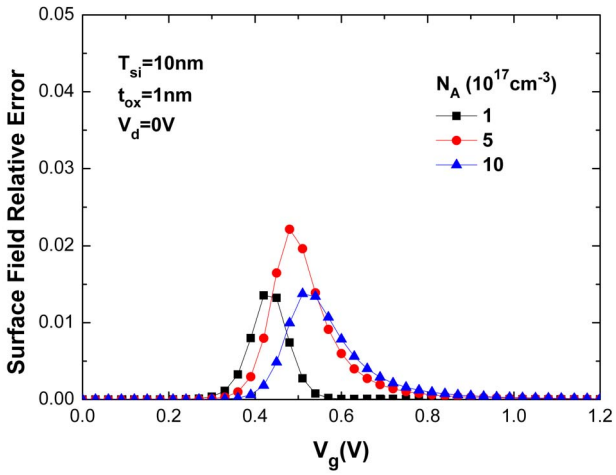

FIGURE 8. **The surface field relative error as a function of V_g for devices with discrete doping profiles.**

Considering the fact that the Dirac function $\delta(x - x_k)$ is just the derivative of the Heaviside step function $H(x - x_k)$, $g(x)$ for a discrete doping profile is:

$$g(x) = \frac{q}{\varepsilon_{si} WL} \sum_{k=1}^{n} N_k x H\,(x - x_k)$$

Hence, the discrete form of function $F(\tau)$ in Eq. (3) can be obtained. Eq. (3) is similar to the discrete 1-D Poisson's equation in the cylindrical coordinate [32]. Following the treatment of [32], Eq. (3) in the discrete form can be solved to calculate the drain current. Note that $p(\tau)$ is a piecewise function for a discrete doping profile, as shown in Figure 2(b). The sum of all discrete charges will match the total amount of depletion charges when assuming a continuous doping profile:

$$\sum_{k=1}^{n} \frac{N_k}{WL} = \int_0^{\frac{T_{si}}{2}} N_a(x)dx = \int_0^{\frac{T_{si}}{2}} N_A dx$$

Therefore, N_A in a discrete model is calculated as:

$$N_A = \frac{\sum_{k=1}^{n} N_k}{\frac{T_{si}}{2} WL}.$$

In Eq. (5), $p(\tau)$ keeps its discrete form during the integration, which provides a useful method to depict the effect of discrete dopant variations. To verify the discrete model accuracy, the relative errors of the surface field of double-gate MOSFETs with varying doping levels are calculated and shown in Figure 8. They exhibit a similar trend to the devices with continuous doping profiles, and the observed maximum error is about 2.8% at an intermediate gate voltage. The surface potentials for devices with discrete doping profile are also plotted and compared with the numerical result in Figure 9. We plot the discrete-model predicted $I_{ds} - V_g$ curves (with varying values of N_A and t_{ox}) of the double-gate MOSFETs in Figure 10. Their good agreement with TCAD

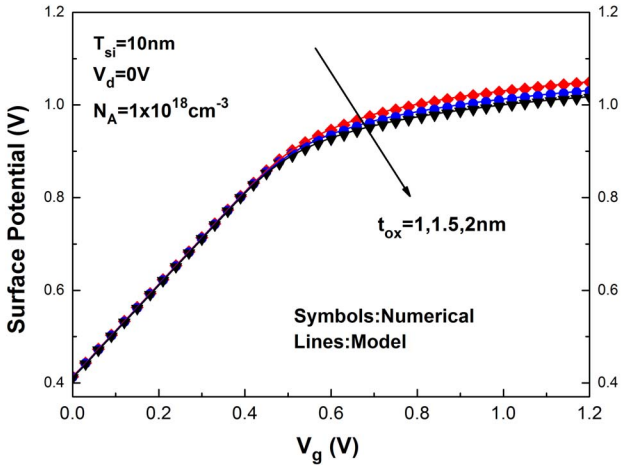

FIGURE 9. **The surface electric potential as a function of V_g for devices with discrete doping profiles.**

simulations indicates the capability of this discrete model to describe the effect of 1-D discrete dopant variations in double-gate MOSFETs.

IV. SHORT-CHANNEL EFFECT

A short-channel-effect (SCE) model for double-gate MOSFETs with continuous and discrete doping profiles will be developed in this section. The short-channel effect for double-gate MOSFETs has been widely studied using various methods [41]–[45]. For instance, in [42], the 2-D potential distribution is assumed as a parabolic function in the radial direction. In [43], the solution of the 2-D Poisson's equation is derived by a conformal mapping approach. By ignoring the inversion charge, 2-D Poisson's equation for the near-threshold operation can be written as:

$$\frac{\partial^2\varphi}{\partial x^2}+\frac{\partial^2\varphi}{\partial y^2}=\frac{qN_a(x,y)}{\varepsilon_{si}}, \tag{27}$$

where $N_a(x,y)$ is the 2-D doping concentration. For a uniform doping profile, $N_a(x,y)=N_A$. For a discrete 2-D doping profile,

$$N_a(x,y)=\sum_{k=1}^{n}\frac{N_k}{W}\delta\left(x-x_k\right)\delta\left(y-y_k\right), \tag{28}$$

and the boundary conditions for Eq. (27) are:

$$\frac{\partial\varphi}{\partial x}\Big|_{x=\frac{t_{si}}{2}}=\frac{C_{ox}}{\varepsilon_{si}}\left(V_g'-\varphi|_{x=\frac{t_{si}}{2}}\right), \tag{29a}$$

$$\varphi|_{y=0}=V_{bi}, \tag{29b}$$

$$\varphi|_{y=L}=V_{bi}+V_d, \tag{29c}$$

where $V_g'=V_g-V_{fb}$ and V_{bi} is the built-in voltage between the channel to the source (drain) junction. By constructing a new variable $\varphi_1=\varphi-V_{bi}-(V_d y)/L$, the boundary condition Eqs. (29b) and (29c) are transformed into the homogeneous form:

$$\varphi_1|_{y=0}=0, \tag{30a}$$

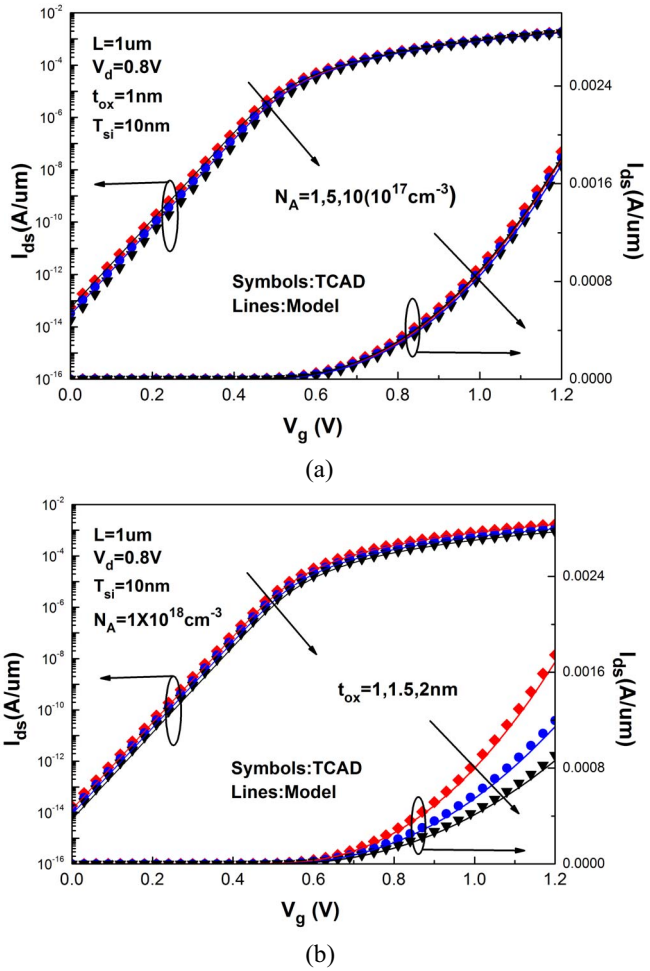

FIGURE 10. **Comparison of $I_{ds}-V_g$ of double-gate MOSFETs with discrete doping profiles based on the new model and the TCAD simulation results for varying (a) N_A, (b) t_{ox}.**

$$\varphi_1|_{y=L}=0. \tag{30b}$$

Eqs. (29a) and (29b) can be reformulated as:

$$\frac{\partial^2\varphi_1}{\partial x^2}+\frac{\partial^2\varphi_1}{\partial y^2}=S(x,y), \tag{31a}$$

$$\frac{\partial\varphi_1}{\partial x}\Big|_{x=\frac{t_{si}}{2}}=\frac{C_{ox}}{\varepsilon_{si}}\left(V_g'-\varphi_1|_{x=\frac{t_{si}}{2}}-V_{bi}-\frac{V_d}{L}y\right), \tag{31b}$$

where $S(x,y)=qN_a(x,y)/\varepsilon_{si}$. Expanding the functions $\varphi_1(x,y)$ and $S(x,y)$ into an infinite series yields:

$$\varphi_1(x,y)=\sum_{t=1}^{+\infty}T_t(x)\sin\left(\omega_t y\right),$$

$$S(x,y)=\sum_{t=1}^{+\infty}S_t(x)\sin\left(\omega_t y\right),$$

where $S_t(x) = 2\int_0^L S(x,y)\sin(\omega_t y)dy/L$ and $\omega_t = t\pi/L$ ($t = 1, 2, 3, \ldots$). Eqs. (31a) and (31b) can be rewritten as:

$$\sum_{t=1}^{+\infty}\left[\frac{d^2}{dx^2}T_t(x) - {\omega_t}^2 T_t(x)\right]\sin(\omega_t y) = \sum_{t=1}^{+\infty} S_t(x)\sin(\omega_t y),$$

$$\sum_{t=1}^{+\infty}\frac{\varepsilon_{si}}{C_{ox}}\frac{d}{dx}T_t(x)|_{x=\frac{t_{si}}{2}}\sin(\omega_t y) = \sum_{t=1}^{+\infty}[\Psi_t - T_t(x)]\sin(\omega_t y),$$

where

$$\Psi_t = \frac{2}{L}\int_0^L \left(V_g{}' - V_{bi} - \frac{V_d}{L}y\right)\sin(\omega_t y)dy.$$

The orthogonal property of $sin(\omega_t y)$ requires [45]:

$$\frac{d^2}{dx^2}T_t(x) - {\omega_t}^2 T_t(x) = S_t(x), \tag{32a}$$

$$\frac{\varepsilon_{si}}{C_{ox}}\frac{d}{dx}T_t(x)\bigg|_{x=\frac{t_{si}}{2}} = \Psi_t - T_t(x)|_{x=\frac{t_{si}}{2}}. \tag{32b}$$

The solution of Eq. (32a) with boundary condition Eq. (32b) is:

$$T_t(x) = C_{1t}e^{\omega_t x} + C_{2t}e^{-\omega_t x} - \phi(x).$$

For the uniform doping distribution,

$$C_{1t} = \frac{\Psi_t + \phi(x)}{\left(1 + \frac{\varepsilon_{si}}{C_{ox}}\omega_t\right)e^{\frac{t_{si}}{2}\omega_t} + \left(1 - \frac{\varepsilon_{si}}{C_{ox}}\omega_t\right)e^{-\frac{t_{si}}{2}\omega_t}},$$

$$C_{2t} = C_{1t},$$

$$\phi(x) = \frac{2qN_A}{\varepsilon_{si}\pi t{\omega_t}^2}[1 - \cos(\pi t)].$$

For the discrete doping profile,

$$C_{1t} = C_{2t} + \sum_{k=1}^{n} A_{kt}e^{-\omega_t x_k},$$

$$C_{2t} = \frac{\Psi_t + D_t}{\left(1 + \frac{\varepsilon_{si}}{C_{ox}}\omega_t\right)e^{\frac{t_{si}}{2}\omega_t} + \left(1 - \frac{\varepsilon_{si}}{C_{ox}}\omega_t\right)e^{-\frac{t_{si}}{2}\omega_t}},$$

$$\phi(x) = \sum_{k=1}^{n} \mathrm{A}_{kt}Exp\left[\omega_t\left(x_{k_<} - x_{k_>}\right)\right],$$

where

$$D_t = \sum_{k=1}^{n} A_{kt}\left\{\left(-\frac{\varepsilon_{si}}{C_{ox}}\omega_t - 1\right)e^{\omega_t\left(\frac{t_{si}}{2} - x_k\right)} + \left(1 - \frac{\varepsilon_{si}}{C_{ox}}\omega_t\right)e^{\omega_t\left(x_k - \frac{t_{si}}{2}\right)}\right\},$$

$$\mathrm{A}_{kt} = \frac{qN_k\sin(\omega_t y_k)}{WL\varepsilon_{si}\omega_t}.$$

$x_{k<}(x_{k>})$ is the smaller (larger) of x and x_k. The subthreshold drain current can be calculated as:

$$I_{ds} = 2\mu WkT\frac{{n_i}^2}{N_a}\frac{e^{-qV_s/kT} - e^{-qV_d/kT}}{\int_0^L \frac{dy}{\int_0^{\frac{t_{si}}{2}} e^{q\varphi(x,y)/kT}dx}}, \tag{33}$$

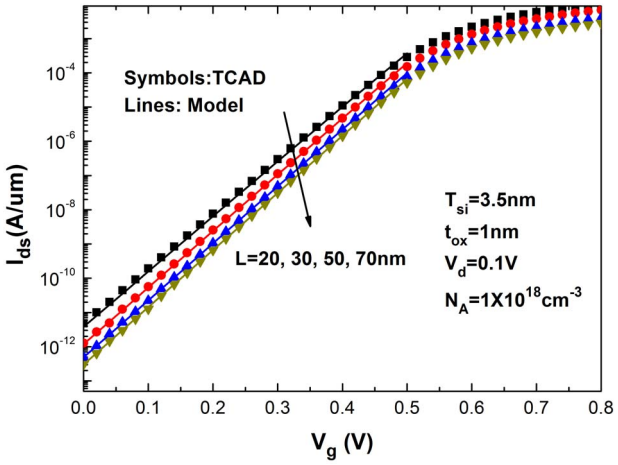

FIGURE 11. **Comparison of the double-gate MOSFET's sub-threshold current predicted by our model and by TCAD simulation when the channel is uniformly doped.**

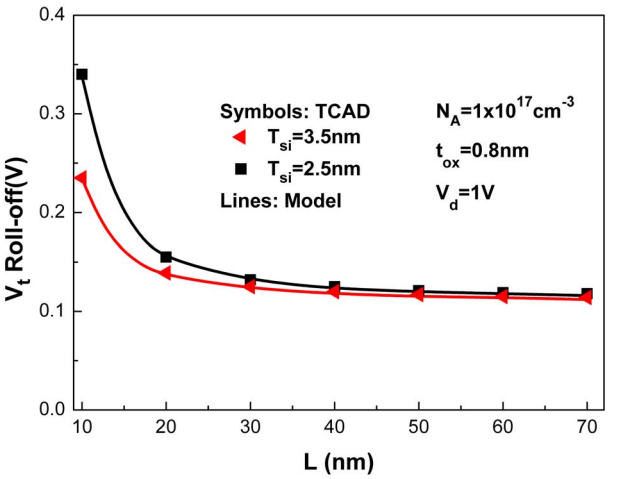

FIGURE 12. **Comparison of the double-gate MOSFET's V_t roll-off predicted by our model and by TCAD simulation when the channel is doped with a uniform doping profile.**

where

$$\varphi(x,y) = \sum_{t=1}^{+\infty} T_t(x)\sin(\omega_t y) + V_{bi} + \frac{V_d}{L}y.$$

The subthreshold current of the double-gate device with uniform doping profiles is first calculated. The corresponding results are compared with those extracted from TCAD simulations as shown in Figure 11. We define V_t roll-off as the V_g shift of a short-channel device relative to the long-channel value at the same current level. Figure 12 shows that the predicted V_t roll-off results are in good agreement with the TCAD simulations for the continuous doping profiles. The threshold voltage V_t is extracted at the gate voltage when the drain current reaches $100(nA/um)\times W/L$. An increase of V_t roll-off with the shrinking channel length shows a further drop of the threshold voltage for shorter device, which is consistent with the trend observed in [41] and [42]. In Figure 13,

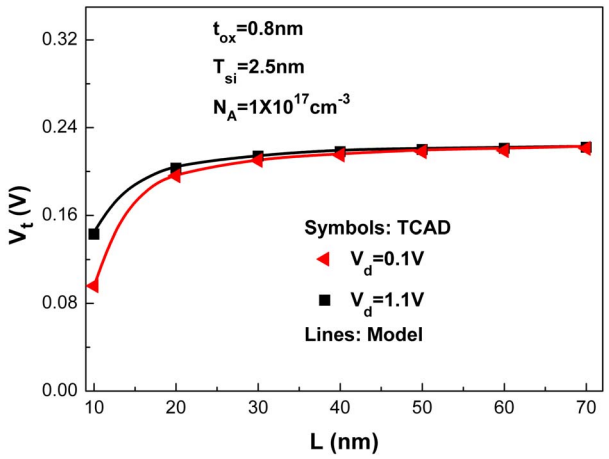

FIGURE 13. Comparison of the double-gate MOSFET's V_t predicted by our model and by TCAD simulation when the channel is doped with discrete doping profile.

V_t values for discrete doping profiles are also extracted and compared with the results of the TCAD simulations. The suppression of the SCE with a lower drain voltage is in agreement with our physical intuition.

V. CONCLUSION

A surface-field based model for double-gate MOSFETs with continuous and discrete (i.e., RDF effects) doping profiles is developed. For discrete doping profiles, the depletion charge is described by multiple Dirac δ functions. Without solving the potential distribution in the channel, an algebraic relation between the electric potential and field is derived from nonlinear 1-D Poisson's equation. It allows us to calculate the drain current with high accuracy. A unified continuous and discrete short-channel model is also developed for double-gate MOSFETs by solving the 2-D Poisson's equation with the eigenfunction-expansion method.

APPENDIX

For a cylindrical MOSFET with an undoped body, Poisson's equation is written as:

$$\frac{d^2Z_C}{d\tau^2}+\frac{1}{\tau}\frac{dZ_C}{d\tau}=\xi_1 e^{Z_C}, \tag{34}$$

where $\xi_1=q^2n_i/(kT\varepsilon_{si})$. By introducing two new variables satisfying: $Z_C=Z-2\ln\tau$ and $\tau=e^x$ [33], Eq. (34) can be rewritten as:

$$\frac{d^2Z}{dx^2}=\xi_1 e^{Z}, \tag{35}$$

Note that Eq. (35) is in the same form as the 1-D Poisson's equation in the Cartesian coordinate. It can be analytically solved and some solution has been reported in double-gate MOSFET compact modeling [8], [9]. Following the derivation in above references, Eq. (35) becomes:

$$\frac{dZ}{dx}=\pm\sqrt{2\xi_1(e^Z+C)}, \tag{36}$$

From the above equation, we obtain a formula of electric field for arbitrary integration constant C. The integration result of its right-hand side depends on the sign of C and multiple branches may possibly exist. In double-gate MOSFET modeling, the branch for $C=0$ was often ignored (e.g., due to the required zero electric field at certain channel location). The complete general solution consists of three different branches [33]:

$$Z=\begin{cases}-2\ln\left|\sin\left[\sqrt{\frac{-C\xi_1}{2}}(x+D)\right]\right| \\ \quad+\ \ln(-C),\ C<0, & (37.1)\\ -2\ln|x+D|+\ln 2-\ln\xi_1,\ C=0, & (37.2)\\ -2\ln\left|\sinh\left[\sqrt{\frac{C\xi_1}{2}}(x+D)\right]\right|+\ln(C),\ C>0. & (37.3)\end{cases}$$

Equation (37.1) corresponds to the solution for symmetric double-gate MOSFETs, while (37.2) - (37.3) are applicable to asymmetric double gate MOSFETs [9].

Using the transformation variables introduced before ($x=\ln\tau$ and $Z=Z_C+2\ln\tau$), the general solution of 1-D cylindrical Poisson's equation can be readily obtained:

$$Z_C=\begin{cases}-2\ln\tau-2\ln\left|\frac{1}{\sqrt{-C}}\sin\left[\sqrt{\frac{-C\xi_1}{2}}(\ln\tau+D)\right]\right|,\ C<0 \\ \qquad\qquad (38.1),\\ -2\ln\tau-2\ln|\ln\tau+D|+\ln 2-\ln\xi_1,\ C=0 \quad (38.2),\\ -2\ln\tau-2\ln\left|\frac{1}{\sqrt{C}}\sinh\left[\sqrt{\frac{C\xi_1}{2}}(\ln\tau+D)\right]\right|,\ C>0 \\ \qquad\qquad (38.3).\end{cases}$$

REFERENCES

[1] D. Hisamoto *et al.*, "FinFET—A self-aligned double-gate MOSFET scalable to 20 nm," *IEEE Trans. Electron Devices*, vol. 47, no. 12, pp. 2320–2325, Dec. 2000.
[2] K. Suzuki, T. Tanaka, Y. Tasaka, H. Horie, and Y. Arimoto, "Scaling theory for double-gate SOI MOSFET's," *IEEE Trans. Electron Devices*, vol. 40, no. 12, pp. 2326–2329, Dec. 1993.
[3] S.-H. Oh, D. Monroe, and J. M. Hergenrother, "Analytic description of short-channel effects in fully-depleted double-gate and cylindrical, surrounding-gate MOSFETs," *IEEE Electron Device Lett.*, vol. 21, no. 9, pp. 445–447, Sep. 2000.
[4] F. Balestra, S. Cristoloveanu, M. Benachir, J. Brini, and T. Elewa, "Double-gate silicon-on-insulator transistor with volume inversion: A new device with greatly enhanced performance," *IEEE Electron Device Lett.*, vol. 8, no. 9, pp. 410–412, Sep. 1987.
[5] D. J. Frank *et al.*, "Device scaling limits of Si MOSFETs and their application dependencies," *Proc. IEEE*, vol. 89, no. 3, pp. 259–288, Mar. 2001.
[6] G. Dessai, A. Deya, G. Gildenblat, and G. D. J. Smit, "Symmetric linearization method for double-gate and surrounding-gate MOSFET models," *Solid State Electron.*, vol. 53, no. 5, pp. 548–556, May 2009.
[7] J.-M. Sallese *et al.*, "A design oriented charge-based current model for symmetric DG MOSFET and its correlation with the EKV formalism," *Solid State Electron.*, vol. 49, no. 3, pp. 485–489, Mar. 2005.
[8] Y. Taur, X. Liang, W. Wang, and H. Lu, "A continuous, analytic drain-current model for DG MOSFETs," *IEEE Electron Device Lett.*, vol. 25, no. 2, pp. 107–109, Feb. 2004.
[9] Y. Taur, "Analytic solutions of charge and capacitance in symmetric and asymmetric double-gate MOSFETs," *IEEE Trans. Electron Devices*, vol. 48, no. 12, pp. 2861–2869, Dec. 2001.
[10] A. Ortiz-Conde, F. J. García-Sánchez, and J. Muci, "Rigorous analytic solution for the drain current of undoped symmetric dual-gate MOSFETs," *Solid State Electron.*, vol. 49, no. 4, pp. 640–647, Apr. 2005.

[11] H. Jin *et al.*, "A non-charge-sheet based analytical model of undoped symmetric double-gate MOSFETs using SPP approach," in *Proc. 5th Int. Symp. Qual. Electron. Design*, San Jose, CA, USA, 2004, pp. 45–50.

[12] F. Liu *et al.*, "Generic carrier-based core model for undoped four-terminal double-gate MOSFETs valid for symmetric, asymmetric, and independent-gate-operation modes," *IEEE Trans. Electron Devices*, vol. 55, no. 3, pp. 816–826, Mar. 2008.

[13] O. Moldovan, D. Jiménez, J. R. Guitart, F. A. Chaves, and B. Iñiguez, "Explicit analytical charge and capacitance models of undoped double-gate MOSFETs," *IEEE Trans. Electron Devices*, vol. 54, no. 7, pp. 1718–1724, Jul. 2007.

[14] M. V. Dunga *et al.*, "Modeling advanced FET technology in a compact model," *IEEE Trans. Electron Devices*, vol. 53, no. 9, pp. 1971–1978, Sep. 2006.

[15] X. Feng, W. Kang, Q. Cheng, and Y. Chen, "An improved compact model for doped double-gate metal–oxide–semiconductor field-effect transistors using a rigorous perturbation method and higher-order correction," *Jpn. J. Appl. Phys.*, vol. 52, no. 4S, Mar. 2013, Art. no. 04CC17.

[16] F. Liu, J. He, J. Zhang, Y. Chen, and M. S. Chan, "A non-charge-sheet analytic model for symmetric double-gate MOSFETs with smooth transition between partially and fully depleted operation modes," *IEEE Trans. Electron Devices*, vol. 55, no. 12, pp. 3494–3502, Dec. 2008.

[17] P. Francis, A. Terao, D. Flandre, and F. Van de Wiele, "Modeling of ultrathin double-gate nMOS/SOI transistors," *IEEE Trans. Electron Devices*, vol. 41, no. 5, pp. 715–720, May 1994.

[18] O. Moldovan *et al.*, "Compact model for highly-doped double-gate SOI MOSFETs targeting baseband analog applications," *Solid State Electron.*, vol. 51, no. 5, pp. 655–661, May 2007.

[19] P. Francis, A. Terao, D. Flandre, and F. Van de Wiele, "Moderate inversion model of ultrathin double-gate nMOS/SOI transistors," *Solid State Electron.*, vol. 38, no. 1, pp. 171–176, Jan. 1995.

[20] J. P. Duarte *et al.*, "A universal core model for multiple-gate field-effect transistors. Part I: Charge model," *IEEE Trans. Electron Devices*, vol. 60, no. 2, pp. 840–847, Feb. 2013.

[21] S. Khandelwal *et al.*, "BSIM-IMG: A compact model for ultrathin-body SOI MOSFETs with back-gate control," *IEEE Trans. Electron Devices*, vol. 59, no. 8, pp. 2019–2026, Aug. 2012.

[22] A. S. Roy, J.-M. Sallese, and C. C. Enz, "A closed-form charge-based expression for drain current in symmetric and asymmetric double gate MOSFET," *Solid State Electron.*, vol. 50, no. 4, pp. 687–693, Apr. 2006.

[23] M. Reyboz, O. Rozeau, T. Poiroux, P. Martin, and J. Jomaah, "An explicit analytical charge-based model of undoped independent double gate MOSFET," *Solid State Electron.*, vol. 50, nos. 7–8, pp. 1276–1282, Jul./Aug. 2006.

[24] W. Z. Shangguan, T. C. A. Yeung, Z. M. Zhu, and X. Zhou, "General analytical Poisson solution for undoped generic two-gated metal-oxide-semiconductor field-effect transistors," *Appl. Phys. Lett.*, vol. 90, no. 1, Jan. 2007, Art. no. 012110.

[25] H. Lu and Y. Taur, "An analytic potential model for symmetric and asymmetric DG MOSFETs," *IEEE Trans. Electron Devices*, vol. 53, no. 5, pp. 1161–1168, May 2006.

[26] B. Diagne, F. Pre'galdiny, C. Lallement, J.-M. Sallese, and F. Krummenacher, "Explicit compact model for symmetric double-gate MOSFETs including solutions for small-geometry effects," *Solid State Electron.*, vol. 52, no. 1, pp. 99–106, Jan. 2008.

[27] F. Liu, L. Zhang, J. Zhang, J. He, and M. Chan, "Effects of body doping on threshold voltage and channel potential of symmetric DG MOSFETs with continuous solution from accumulation to strong-inversion regions," *Semicond. Sci. Technol.*, vol. 24, no. 8, pp. 1–8, Aug. 2009.

[28] A. Yesayan, F. Prégaldiny, N. Chevillon, C. Lallement, and J.-M. Sallese, "Physics-based compact model for ultra-scaled FinFETs," *Solid State Electron.*, vol. 61, no. 1, pp. 165–173, Aug. 2011.

[29] D. D. Lu, M. V. Dunga, C.-H. Lin, A. M. Niknejad, and C. Hu, "A multi-gate MOSFET compact model featuring independent-gate operation," in *IEDM Tech. Dig.*, Washington, DC, USA, 2007, pp. 565–568.

[30] G. Pei, W. Ni, A. V. Kammula, B. A. Minch, and E. C.-C. Kan, "A physical compact model of DG MOSFET for mixed-signal circuit applications—Part I: Model description," *IEEE Trans. Electron Devices*, vol. 50, no. 10, pp. 2135–2143, Oct. 2003.

[31] Q. Cheng, C. Hong, J. B. Kuo, and Y. Chen, "A surface-field-based model for nanowire MOSFETs with spatial variations of doping profiles," *IEEE Trans. Electron Devices*, vol. 61, no. 12, pp. 4040–4046, Dec. 2014.

[32] C. Hong *et al.*, "An analytic surface-field-based quasi-atomistic model for nanowire MOSFETs with random dopant fluctuations," *IEEE Trans. Electron Devices*, vol. 62, no. 12, pp. 4179–4185, Dec. 2015.

[33] J. Zhou, "On compact model for double-surrounding-gate MOSFETs and the yield study of lithographic processes," Ph.D. dissertation, School Electron. Comput. Eng., Peking Univ., Beijing, China, 2016.

[34] C. Hong *et al.*, "A continuous compact model incorporating higher-order correction for junctionless nanowire transistors with arbitrary doping profiles," *IEEE Trans. Nanotechnol.*, vol. 15, no. 4, pp. 657–665, Jul. 2016.

[35] J.-M. Sallese, N. Chevillon, F. Prégaldiny, C. Lallement, and B. Iñiguez, "The equivalent-thickness concept for doped symmetric DG MOSFETs," *IEEE Trans. Electron Devices*, vol. 57, no. 11, pp. 2917–2924, Nov. 2010.

[36] Y. Taur, H.-P. Chen, W. Wang, S.-H. Lo, and C. Wann, "On–off charge–voltage characteristics and dopant number fluctuation effects in junctionless double-gate MOSFETs," *IEEE Trans. Electron Devices*, vol. 59, no. 3, pp. 863–866, Mar. 2012.

[37] Y. Taur and T. H. Ning, *Fundamentals of Modern VLSI Devices*. Cambridge, U.K.: Cambridge Univ. Press, 1998, pp. 78–85 and pp. 210–240.

[38] L. Dunlop, "An efficient mosfet current model for analog circuit simulation-subthreshold to strong inversion," *IEEE J. Solid-State Circuits*, vol. 25, no. 2, pp. 616–619, Apr. 1990.

[39] (Oct. 2105). *Mathematica 10.1*. [Online]. Available: http://www.wolfram.com/

[40] *Sentaurus User Guide, Version A-2008.09*, Synopsys Inc., Mountain View, CA, USA, Sep. 2008.

[41] X. Liang and Y. Taur, "A 2-D analytical solution for SCEs in DG MOSFETs," *IEEE Trans. Electron Devices*, vol. 51, no. 9, pp. 1385–1391, Sep. 2004.

[42] K. Suzuki, Y. Tosaka, and T. Sugii, "Analytical threshold voltage model for short channel double-gate SOI MOSFETs," *IEEE Trans. Electron Devices*, vol. 43, no. 7, pp. 1166–1168, Jul. 1996.

[43] H. Børli, S. Kolberg, T. A. Fjeldly, and B. Iñíguez, "Precise modeling framework for short-channel double-gate and gate-all-around MOSFETs," *IEEE Trans. Electron Devices*, vol. 55, no. 10, pp. 2678–2686, Oct. 2008.

[44] Q. Chen, E. M. Harrell, II, and J. D. Meindl, "A physical short-channel threshold voltage model for undoped symmetric double-gate MOSFETs," *IEEE Trans. Electron Devices*, vol. 50, no. 7, pp. 1631–1637, Jul. 2003.

[45] S. Hassani, *Mathematical Physics: A Modern Introduction to Its Foundations*. New York, NY, USA: Springer, 1999, pp. 551–641.

CHUYANG HONG received the B.S. degree from the Guangdong University of Technology, China, in 2013. He is currently pursuing the M.S. degree in microelectronics with the School of Electronic and Computer Engineering, Peking University (Shenzhen Graduate School), Shenzhen, China.

JUN ZHOU received the B.S. degree from Jiangnan University, China, in 2013. He is currently pursuing the M.S. degree in microelectronics with the School of Electronic and Computer Engineering, Peking University (Shenzhen Graduate School), Shenzhen, China. His research interests include yield model of lithography and device modeling.

QI CHENG received the B.S. degree from the Huazhong University of Science and Technology, China, in 2011, and the M.S. degree in microelectronics from the School of Electronic and Computer Engineering, Peking University (Shenzhen Graduate School), Shenzhen, China. He is currently a Research Assistant working on the sub-10-nm process variability-related device modeling and circuit simulation.

KUNKUN ZHU received the B.S. degree from the China University of Mining and Technology, Xuzhou, China. He is currently pursuing the M.S. degree in microelectronics with the School of Electronic and Computer Engineering, Peking University Shenzhen Graduate School, Shenzhen, China.

JAMES B. KUO (S'85–M'85–SM'92–F'00) received the B.S.E.E. degree from National Taiwan University, Taipei, Taiwan, the M.S.E.E. degree from Ohio State University, Columbus, OH, USA, and the Ph.D. degree from Stanford University, Stanford, CA, USA. He is currently a Professor with the Department of Electrical Engineering, National Taiwan University. His current research interests include low-voltage CMOS circuits and compact modeling of SOI CMOS devices.

YIJIAN CHEN (S'00–M'05) received the B.S. degree from Peking University, Beijing, China, the M.S. degree from the Massachusetts Institute of Technology, Cambridge, MA, USA, and the Ph.D. degree from the University of California at Berkeley, Berkeley, CA, USA. He is currently an Associate Professor with the School of Electronic and Computer Engineering, Peking University (Shenzhen Graduate School), China.